# Supporting information to Non-Boltzmann Luminescence in $NaYF_4:Eu^{3+}$: Implications for Luminescence Thermometry

Robin G. Geitenbeek, Harold W. de Wijn, Andries Meijerink

## Experimental section

Microcrystalline $NaYF_4$ was prepared via a solid state synthesis.[32] In short, 15 mmol of NaF, 15 mmol of $REF_3$ (RE = Y, Eu) and 13.5 mmol of $NH_4F$ were mixed with a pestle and mortar and afterwards placed in an alumina crucible. The mixture was fired in the oven in an excess of $NH_4F$ under a nitrogen atmosphere. The samples were heated to 300 °C for 3 h and afterwards heated to 550 °C for 8 h. The heating rate was 5 °C $min^{-1}$ for both heating steps.
After synthesis, the samples were crushed with a pestle and mortar and the crystallinity was confirmed with x-ray diffraction measurements using a Philips PW1729 x-ray diffractometer. To remove the NaF impurities, samples were dispersed in $H_2O$ and after dissolving the NaF the samples were centrifuged, decantated and dried to remove the $H_2O$.
The synthesis product was analyzed using scanning electron microscopy (SEM), powder X-ray diffraction (XRD) and inductively coupled plasma optical emission spectroscopy (ICP-OES). The as-synthesized particles were micrometer sized and mainly hexagonal $NaYF_4$ as shown in Figs. S1 and S2. The NaF impurities were successfully removed by washing with $H_2O$ as shown in Fig. S2. The $Eu^{3+}$ dopant concentrations, determined with ICP-OES, are 0.4%, 5.5% and 8.4% for the three different samples. The low dopant sample (0.4% $Eu^{3+}$) is used for the main part of the work while the two higher concentration samples are used to investigate the role of cross-relaxation measurements.
Luminescence measurements were performed using a 5 mW 405 ± 10 nm diode laser and an Ocean Optics QE Pro010451 CCD. Luminescence decay measurements were measured with an Ekspla NT 342B tunable laser, a Triax 550 single emission monochromator, a Hamamatsu R928 PMT and a EG&G Ortec Turbo-MCS multichannel scaler.

## Cross-relaxation

In order to expand the temperature range of luminescence thermometry with $Eu^{3+}$ to lower temperatures, it is desirable to enhance the relaxation rate between the $^5D_1$ and $^5D_0$ levels. A potential mechanism to induce additional relaxation in this system is cross-relaxation, radiationless energy transfer between neighboring ions having resonant, or nearly resonant, transitions. A prerequisite is that the dopant concentration is sufficiently high for the dopant ions to interact.
In $NaYF_4:Eu^{3+}$, cross-relaxation is possible since the energy of ca. 1800 $cm^{-1}$ released in a radiationless transition from $^5D_1$ to $^5D_0$ may be transferred to a neighboring $Eu^{3+}$ ion residing in the $^7F_0$ ground state, resulting in a transition to the $^7F_3$ state at approximately 1800 $cm^{-1}$. The residual energy from the mismatch between the two different transitions is compensated by the emission or absorption of a low-energy acoustic phonon. At higher temperatures, the $^7F_3$ level becomes thermally accessible and therefore the reverse process becomes relevant as well. Additionally, the transition between the $^7F_2$ and $^7F_4$ levels involves approximately the same energy (ca. 1800 $cm^{-1}$) and can also contribute to the cross-relaxation processes once the $^7F_2$ and $^7F_4$ levels are thermally accessible. Note that although the $^7F_2$ and $^7F_4$ levels become accessible at a higher temperature than the $^7F_0$ and $^7F_3$ levels, the transition matrix elements connecting the $^7F_2$ and $^7F_4$ levels are larger due to the favorable $\Delta J$ value of 2. Based on Judd-Ofelt theory the transition probabilities for $\Delta J$ = 0, 2, 4 or 6 (not 0–0) transitions are possible as forced electric dipole transition while the $\Delta J$ = 3 ($^7F_0$–$^7F_3$) transition is not.[2] The reduced matrix elements $U^{(\lambda)}$ are all zero for the $^7F_0$–$^7F_3$ transition, while the matrix elements are large for the $^7F_2$–$^7F_4$ transition ($U^{(2)2}$ = 0.2226, $U^{(4)2}$ = 0.0062 and $U^{(6)2}$ = 0.0329).[21] Typically, forced electric dipole transitions ($\Delta J$ = 0, 2, 4 or 6) are an order of magnitude stronger than other *J*–*J* transitions which makes cross-relaxation involving the $^7F_2$–$^7F_4$ transition favorable once these levels are thermally populated.
Cross-relaxation depends on the distribution of the $Eu^{3+}$ ions over the lattice, notably the presence of nearest and next-nearest neighbors. A configuration of $Eu^{3+}$ neighbors thus gives rise to a specific cross-relaxation rate that will vary for different $Eu^{3+}$ ions. Faster cross-relaxation will occur for $Eu^{3+}$

ions with one (or more) nearest $Eu^{3+}$ neighbors. This will result in a multi-exponential decay. This is observed for samples with higher $Eu^{3+}$ dopant levels of 5.5% and 8.4% as shown in Figs. S3 and S4. However, if the total luminescence is monitored via steady-state measurements, the temporal dependence of the various relaxation processes are averaged out and the intensity variations can be analyzed using an effective temperature-dependent cross-relaxation rate.

To explore the effect of the $Eu^{3+}$ dopant concentration on the temperature-dependent $^5D_1/^5D_0$ intensity ratio, the luminescence of two samples with a higher $Eu^{3+}$ dopant concentration, 5.5% and 8.4%, have been measured as shown in Fig. S5. From the spectra, the fluorescence intensity ratio of the $^5D_1$ and $^5D_0$ level has been calculated for temperatures ranging from 300–900 K and are shown in Fig. 5.

To model the cross-relaxation effects, we rewrite Eq. (12) to include

$$X_1 = g_1(X_{03}N_0' + X_{24}N_2') \qquad \text{(S1)}$$

and

$$X_2 = g_2(X_{03}N_3' + X_{24}N_4'). \qquad \text{(S2)}$$

Here, $X_{03}$ and $X_{24}$ contain the relevant matrix elements for the transitions between the $^7F_0$–$^7F_3$ and $^7F_2$–$^7F_4$ respectively and the populations of the $^7F_J$ states (having energy $E_J$) of the neighboring $Eu^{3+}$ ions, $N_J'$ is given by

$$N_J' = N'(2J+1)\frac{\exp(-E_J/kT)}{Z}, \qquad (S3)$$

in which $N$' measures the density of adjacent $Eu^{3+}$ contributing to cross-relaxation and Z is the state sum. Note that we assume here that the energy of the $^7F_J$ levels ($E_J$) is not affected by interactions with the neighboring $Eu^{3+}$ ion in the $^5D_0$ or $^5D_1$ level. The phonon processes to compensate for the energy mismatch during cross-relaxation are also assumed to be much faster than cross-relaxation and are therefore omitted from Eqs. (S1) and (S2).

To quantify the added effect of cross-relaxation in Fig. 5, the data from the 5.5% (red) and 8.4% (orange) sample were fitted using equation Eq. (12) with Eqs. (S1) and (S2). In the fitting procedure all obtained fitting parameters from the 0.4% sample (blue) were maintained, resulting in only 2 additional fitting parameters, $X_{03}$ and $X_{24}$. The model with obtained values, ($X_{03} = 0.41 \pm 0.05$ ms$^{-1}$ and $X_{24} = 4.0 \pm 0.4$ ms$^{-1}$ for the 5.5% $Eu^{3+}$ concentration and $X_{03} = 0.75 \pm 0.10$ ms$^{-1}$ and $X_{24} = 9.7 \pm 1.4$ ms$^{-1}$ for the 8.4% $Eu^{3+}$ concentration) fits the data very well.

The $^7F_2$–$^7F_4$ transition has a transition probability for cross-relaxation that is larger by an order of magnitude in comparison with the $^7F_0$–$^7F_3$ transition. This is in line with the forced electric dipole character of the $^7F_2$–$^7F_4$ transition. In fact, at elevated temperatures $^7F_2$–$^7F_4$ is more effective, taking over from $^7F_0$–$^7F_3$ above ca. 400 K as the dominant cross-relaxation process. We furthermore see that cross-relaxation rates increase roughly linearly with the $Eu^{3+}$ concentration which is expected as the average number of $Eu^{3+}$ neighbors increases linearly with $Eu^{3+}$ concentration.

The experiments on the higher-doped $Eu^{3+}$ samples have provided evidence that the temperature dependence of the $^5D_1/^5D_0$ intensity ratio is strongly influenced by the $Eu^{3+}$ concentration. At higher concentrations, the temperature dependence of the $^5D_1/^5D_0$ intensity ratio can be used to probe temperatures above ca. 500 K. The useful temperature range for luminescence thermometry can thus be controlled and extended through the dopant concentration. The dopant concentration is identified as an important parameter in the performance of (nano)thermometers based on lanthanide-doped luminescent materials, and the temperature regime in which Boltzmann equilibrium is reached.

## Figures and Tables

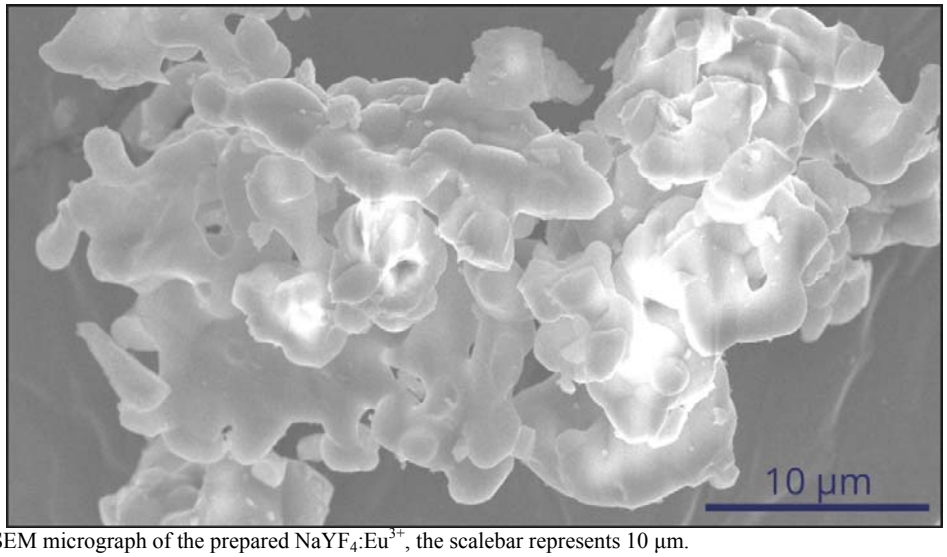


FIG. S1. SEM micrograph of the prepared $NaYF_4:Eu^{3+}$, the scalebar represents 10 µm.

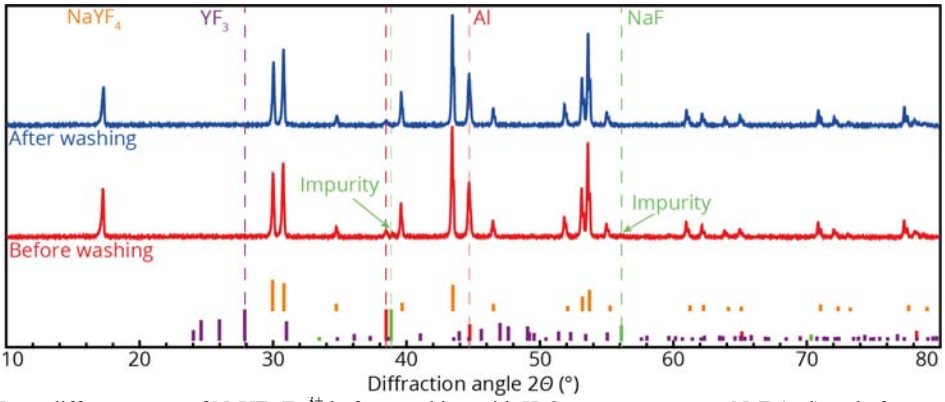


FIG. S2. X-ray diffractograms of $NaYF_4:Eu^{3+}$ before washing with $H_2O$ to remove excess NaF (red) and after washing with $H_2O$ (blue). The reference diffractograms include $NaYF_4$ (JCPDS00-064-0156, orange), $YF_3$ (JCPDS04-007-0883, purple), NaF (JCPDS00-036-1455, green) and aluminium from the sample holder (JCPDS00-004-0787, red). The dashed lines represent angles where the major diffraction peaks of the references are expected.

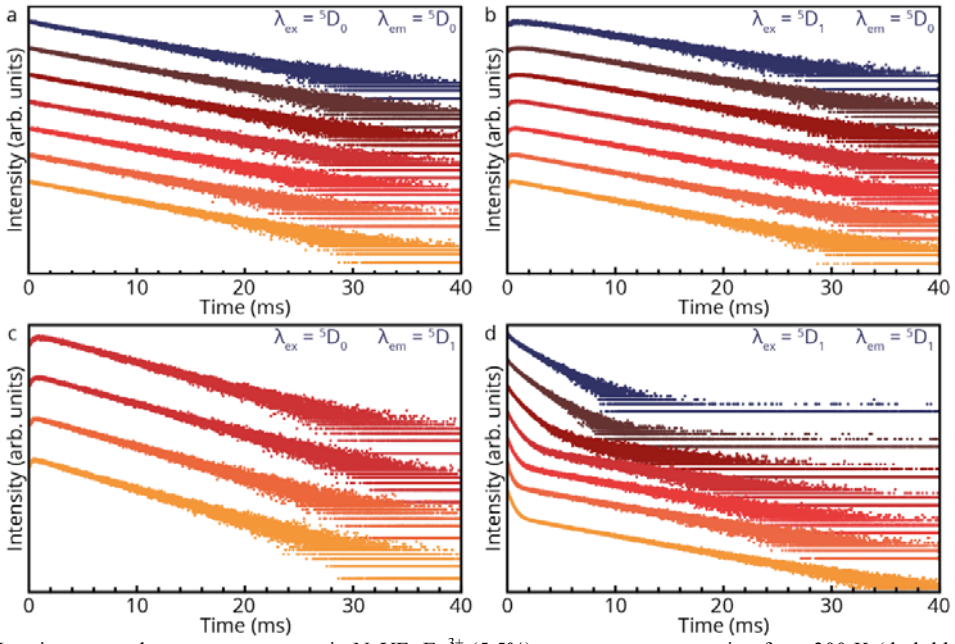


FIG. S3. Luminescence decay measurements in $NaYF_4:Eu^{3+}$ (5.5%) at temperatures ranging from 300 K (dark blue) to 900 K (orange) while exciting in the $^5D_0$ and $^5D_1$ state and monitoring the $^5D_0$ level (a and b respectively) and while exciting in the $^5D_0$ and $^5D_1$ level and monitoring the $^5D_1$ level (c and d respectively).

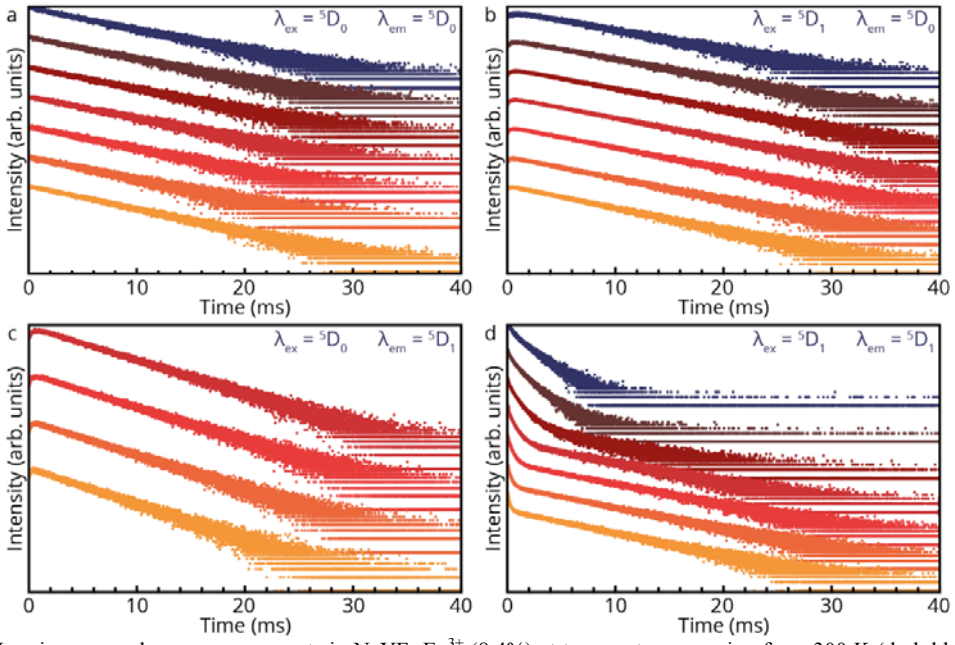


FIG. S4. Luminescence decay measurements in $NaYF_4:Eu^{3+}$ (8.4%) at temperatures ranging from 300 K (dark blue) to 900 K (orange) while exciting in the $^5D_0$ and $^5D_1$ state and monitoring the $^5D_0$ level (a and b respectively) and while exciting in the $^5D_0$ and $^5D_1$ level and monitoring the $^5D_1$ level (c and d respectively).

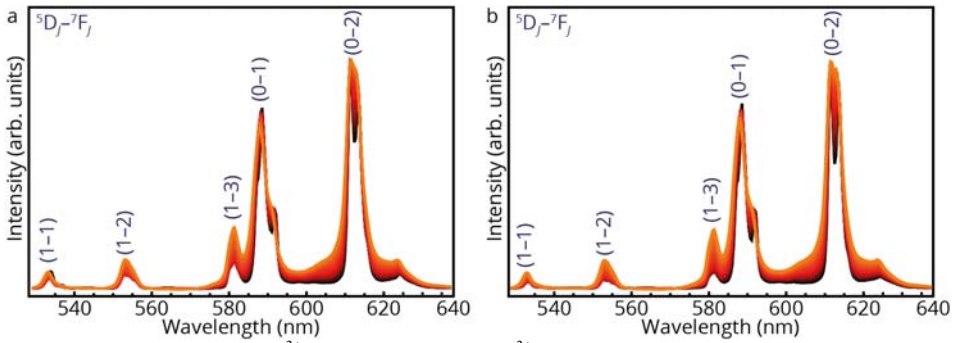


FIG. S5. Emission spectra of $NaYF_4:Eu^{3+}$ (5.7%) and $NaYF_4:Eu^{3+}$ (8.4%) (a,b resp.) upon excitation at 405 nm taken at different temperatures ranging from 300 K (black) to 900 K (orange).

TABLE SI. Fitted lifetimes ($\tau_1$ and $\tau_2$) of the decay measurements of the $^5D_0$ state upon excitation in the $^5D_0$ state and the corresponding radiative ($\tau_R$) and non-radiative lifetimes ($\tau_{NR}$).

| | **300 K** | **373 K** | **473 K** | **573 K** | **673 K** | **773 K** | **873 K** |
|---|---|---|---|---|---|---|---|
| **$1/r_1$ (ms)** | 6.2 | 6.2 | 6.1 | 6.0 | 5.9 | 5.8 | 5.9 |
| **$1/r_2$ (ms)** | 2.2 | 2.0 | 1.6 | 1.3 | 1.0 | 0.5 | 0.5 |
| **$\tau_R$ (ms)** | 6.2 | 6.2 | 6.1 | 6.0 | 5.9 | 5.8 | 5.9 |
| **$\tau_{NR}$ (ms)** | 3.4 | 3.0 | 2.3 | 1.7 | 1.2 | 0.5 | 0.6 |

TABLE SII. Fitted lifetimes ($\tau_1$ and $\tau_2$) of the decay measurements of the $^5D_0$ state upon excitation in the $^5D_1$ state and the corresponding radiative ($\tau_R$) and non-radiative lifetimes ($\tau_{NR}$).

| | **300 K** | **373 K** | **473 K** | **573 K** | **673 K** | **773 K** | **873 K** |
|---|---|---|---|---|---|---|---|
| **$1/r_1$ (ms)** | 6.3 | 6.4 | 6.2 | 6.1 | 5.9 | 5.8 | 5.9 |
| **$1/r_2$ (ms)** | 2.0 | 1.5 | 1.1 | 0.7 | 0.5 | 0.3 | 0.3 |
| **$\tau_R$ (ms)** | 6.3 | 6.4 | 6.2 | 6.1 | 5.9 | 5.8 | 5.9 |
| **$\tau_{NR}$ (ms)** | 3.0 | 2.0 | 1.3 | 0.8 | 0.5 | 0.3 | 0.3 |

TABLE SIII. Fitted lifetimes ($\tau_1$ and $\tau_2$) of the decay measurements of the $^5D_1$ state upon excitation in the $^5D_0$ state and the corresponding radiative ($\tau_R$) and non-radiative lifetimes ($\tau_{NR}$).

| | **300 K** | **373 K** | **473 K** | **573 K** | **673 K** | **773 K** | **873 K** |
|---|---|---|---|---|---|---|---|
| **$1/r_1$ (ms)** | - | - | - | 6.1 | 5.9 | 5.8 | 5.9 |
| **$1/r_2$ (ms)** | - | - | - | 0.7 | 0.5 | 0.3 | 0.3 |
| **$\tau_R$ (ms)** | - | - | - | 6.1 | 5.9 | 5.8 | 5.9 |
| **$\tau_{NR}$ (ms)** | - | - | - | 0.8 | 0.6 | 0.4 | 0.4 |

TABLE SIV. Fitted lifetimes ($\tau_1$ and $\tau_2$) of the decay measurements of the $^5D_1$ state upon excitation in the $^5D_1$ state and the corresponding radiative ($\tau_R$) and non-radiative lifetimes ($\tau_{NR}$).

| | **300 K** | **373 K** | **473 K** | **573 K** | **673 K** | **773 K** | **873 K** |
|---|---|---|---|---|---|---|---|
| **$1/r_1$ (ms)** | 6.2 | 6.2 | 6.1 | 6.0 | 5.8 | 5.6 | 5.8 |
| **$1/r_2$ (ms)** | 2.3 | 1.8 | 1.2 | 0.8 | 0.5 | 0.3 | 0.3 |
| **$\tau_R$ (ms)** | 6.2 | 6.2 | 6.1 | 6.0 | 5.8 | 5.6 | 5.8 |
| **$\tau_{NR}$ (ms)** | 3.7 | 2.5 | 1.5 | 0.9 | 0.6 | 0.4 | 0.4 |

In the fits, the consecutive photon-counting bins were weighed according to Poisson statistics, with appropriate account for low-count bins.